Journal of Applied Physics ARTICLE scitation.org/journal/jap

First-principles study of electronic, optical and thermal transport properties of group III–VI monolayer MX (M = Ga, In; X = S, Se)

Cite as: J. Appl. Phys. **125**, 245104 (2019); doi: 10.1063/1.5094663
Submitted: 4 March 2019 · Accepted: 3 June 2019 ·
Published Online: 25 June 2019

Huimin Wang,[1,2,a)] Guangzhao Qin,[3,a)] Jiayue Yang,[4] Zhenzhen Qin,[5] Yagang Yao,[2] Qiang Wang,[1,b)] and Ming Hu[3,b)]

AFFILIATIONS

[1]Key Laboratory of Electromagnetic Processing of Materials (Ministry of Education), Northeastern University, 110819 Shenyang, China
[2]College of Engineering and Applied Science, Nanjing University, Nanjing 210023, China
[3]Department of Mechanical Engineering, University of South Carolina, Columbia, South Carolina 29209, USA
[4]School of Energy and Power Engineering, Shandong University, Qingdao 266237, China
[5]International Laboratory for Quantum Functional Materials of Henan and School of Physics and Engineering, Zhengzhou University, Zhengzhou 450001, China

[a)]**Contributions:** H. Wang and G. Qin contributed equally to this work.
[b)]**Authors to whom correspondence should be addressed:** wangq@mail.neu.edu.cn and hu@sc.edu

ABSTRACT

Two-dimensional (2D) GaS, GaSe, and InSe were reported to be semiconductors and have been recently fabricated with potential applications in photoelectrics, where in-depth understanding from electronic structure is necessary. In addition, the thermal transport properties play a key role as to the thermal stability and the efficient heat dissipation for device operation, which are also necessary to be addressed. In this paper, we present a systematic first-principles study on the electronic, optical, and thermal transport properties for the representative group III–VI monolayer GaS, GaSe, and InSe. Our results indicate that monolayer GaS, GaSe, and InSe are semiconductors with an indirect bandgap. The predominant influence of interband transitions due to the large bandgap causes monolayer GaSe to possess the highest absorptivity along both "in-plane" and "out-of-plane" directions compared to the other two systems. Moreover, the lattice thermal conductivities (κ_L) of these materials are found to be inversely proportional to their average atomic mass, but the decrease in thermal conductivity from GaS to GaSe is negligible in comparison to that of GaSe to InSe with a nearly equivalent mass difference. It is found that the underlying mechanism lies in the larger phonon relaxation time of GaSe caused by weaker anharmonicity. Our study provides a comprehensive understanding of the inherent physical properties of monolayer GaS, GaSe, and InSe, which would benefit their future applications in photoelectrics.

I. INTRODUCTION

Since the successful exfoliation of graphene, two-dimensional nanomaterials including van der Waals layered transition metal dichalcogenides, phosphorene, and silicene have received growing interest due to their astonishingly novel characteristics compared with their bulk structures for the potential application in electronics and optoelectronics.[1–5] Unlike gapless graphene that restricts its application in electronic devices, several 2D metal chalcogenides present obvious electric bandgap, which can be tuned by changing composition, thickness, and mechanical strain.[6] III–VI layered compounds like GaS, GaSe, and InSe in a hexagonal structure have received more attention due to the potential application in solar energy conversion, nonlinear optics, terahertz generation, and memory devices.[7,8] Since bulk GaS, InSe, and GaSe are semiconductors, their electronic states could allow the photoelectronic carriers to be generated compared to gapless graphene.[9,10] From the experiment, monolayer GaS, GaSe, and InSe have already been successfully fabricated by mechanical exfoliation,[11,12] chemical vapor deposition,[13] pulsed laser deposition,[14]

and colloidal ligand template methods.[15] Applications of these monolayer materials fundamentally depend on their inherent physical nature. Behaviors of microscopic electrons influence lattice vibration, which is related to optical absorption and also influence the thermal transport property of materials. The dielectric function is a fundamental thermophysical property, which can provide the optical absorption characterization and is intrinsically related to the electronic intraband and interband transitions.[16–18] Thermal transport properties play a crucial role in determining the stability of electronic devices and the efficiency of thermoelectric devices. In an earlier experiment, a low thermal conductivity ($\kappa_L < 1.2\ \mathrm{W\,m^{-1}\,K^{-1}}$) at room temperature was reported in the bulk InSe crystal.[19,20] While due to the state and size of the sample, the intrinsic parameters could be different from experimental characterization. As such, the comprehensive research of inherent physical characters is necessary and beneficial for the device applications of these monolayer materials.

In this paper, we systematically studied the intrinsic electronic, optical, and thermal transport properties of monolayer GaS, GaSe, and InSe. The absorption peaks along "in-plane" and "out-of-plane" directions are attributed to the upper valence band to conduction band transitions except for the highest peaks in monolayer GaS and InSe and the second highest peak in GaSe along the out-of-plane direction since these are attributed to intraband transitions. GaS possesses the largest absorptivity contributed by interband transitions. The decreasing κ_L along with increasing average atomic mass makes InSe present the lowest κ_L ($2.69\ \mathrm{W\,m^{-1}\,K^{-1}}$), which is consistent with the experimental values.[19] Considering the almost equal mass difference, the small difference of κ_L between GaS and GaSe ($0.91\ \mathrm{W\,m^{-1}\,K^{-1}}$) compared to the decreased κ_L from GaSe to InSe ($10.66\ \mathrm{W\,m^{-1}\,K^{-1}}$) is due to the larger phonon relaxation time of GaSe caused by its weaker anharmonicity. This research could provide a fundamental theoretical understanding for the experimental characterization of these materials.

II. COMPUTATIONAL METHODOLOGY

All the first-principles calculations based on the density functional theory (DFT) were carried out by Vienna *ab initio* simulation package (VASP).[21–23] For all calculations, we used the projector augmented wave (PAW) method[24,25] and chose the Perdew-Burke-Ernzerhof (PBE) of generalized gradient approximation (GGA) as the exchange-correlation functional. For high precision, large kinetic energy cutoffs were set to ~2.5 times the maximal recommended cutoff in the pseudopotentials, namely, 1000, 520, and 598 eV for monolayer GaS, GaSe, and InSe, respectively. To prevent the influence of interactions between periodic layers, a vacuum spacing of 20 Å was used along the out-of-plane (z) direction. The energy convergence threshold was set at 10^{-6} eV. The unit cell was optimized with a $31 \times 31 \times 1$ Monkhorst-Pack[26] k-point mesh, along with the Hellmann-Feynman force convergence threshold set as 1×10^{-7} eV/Å.

A $31 \times 31 \times 1$ Monkhorst-Pack k-point was used for the calculation of optical properties. The optical properties can be derived from the frequency-dependent dielectric function $\varepsilon(\omega) = \varepsilon_1(\omega) + i\varepsilon_2(\omega)$. Based on Fermi's golden rule, the imaginary part $\varepsilon_2(\omega)$ can be obtained by[27]

$$\varepsilon_2(\omega) = \frac{4\pi^2 e^2}{m^2\omega^2} \times \sum_{C,V} |P_{C,V}|^2 \delta(E_C - E_V - \hbar\omega), \tag{1}$$

where e is the electron charge, m is the effective mass, ω is the angular frequency, and C and V represent the conduction band and valence band, respectively. In addition, P denotes the momentum transition matrix, E is the electron energy level, and $\hbar$ is Planck's constant. The function δ ensures the conversion of energy during electrons transit from band to band. Due to the presence of the vacuum layer, the calculated dielectric function should be normalized to its 100% volume fraction as[17]

$$\langle\varepsilon_2\rangle = \frac{L}{d}\varepsilon_2, \tag{2}$$

where L is the separation distance between the isolated layers and d is the layer thickness. The normalized real part $\langle\varepsilon_1\rangle$ can be calculated from $\langle\varepsilon_2\rangle$ by the Kramers-Kronig dispersion relation,[28]

$$\langle\varepsilon_1(\omega)\rangle = 1 + \frac{2}{\pi}\int_0^\infty \frac{\omega'\langle\varepsilon_2(\omega')\rangle}{\omega'^2 - \omega^2}\, d\omega'. \tag{3}$$

Based on the dielectric function, the reflection index $n(\omega)$ and the extinction coefficient $k(\omega)$ are expressed as

$$n(\omega) = \frac{1}{\sqrt{2}}\left[\sqrt{\varepsilon_1(\omega)^2 + \varepsilon_2(\omega)^2} + \varepsilon_1(\omega)\right]^{\frac{1}{2}}, \tag{4}$$

$$k(\omega) = \frac{1}{\sqrt{2}}\left[\sqrt{\varepsilon_1(\omega)^2 + \varepsilon_2(\omega)^2} - \varepsilon_1(\omega)\right]^{\frac{1}{2}}. \tag{5}$$

The optical reflectivity $R(\omega)$ and the absorption coefficient $\alpha(\omega)$ are obtained with calculated $n(\omega)$ and $k(\omega)$ by

$$R(\omega) = \frac{[n(\omega) - 1]^2 + k(\omega)^2}{[n(\omega) + 1]^2 + k(\omega)^2}, \tag{6}$$

$$\alpha(\omega) = \frac{2\omega k(\omega)}{c} = \frac{\varepsilon_2(\omega)\omega}{n(\omega)c}, \tag{7}$$

where c is the speed of light.

With a $2 \times 2 \times 1$ Monkhorst-Park k-mesh, a $4 \times 4 \times 1$ supercell was built to calculate the harmonic and anharmonic interatomic force constants (IFCs), which are obtained based on the second and third order derivatives of the total energy, respectively. The cutoff distances (rcutoff) corresponding to anharmonic IFCs are 4.5, 4.7, and 4.8 Å, and the thicknesses are 8.712, 8.875, and 8.775 Å for GaS, GaSe, and InSe, respectively. Based on the density functional perturbation theory (DFPT), Born effective charges and dielectric permittivity tensor are obtained to correct the dynamical matrix for considering long-ranged electrostatic interactions. By iteratively solving the linearized phonon Boltzmann transport equation (BTE), the lattice thermal conductivity is calculated as implemented in ShengBTE package[29] and can be formulated as

$$\kappa^{\alpha\beta} = \frac{1}{k_B T^2 N\Omega}\sum_\lambda f_0(f_0 + 1)(\hbar\omega_\lambda)^2 v_\lambda^\alpha F_\lambda^\beta, \tag{8}$$

where k_B is the Boltzmann constant and Ω is the volume of the unit cell. ω_λ is the angular frequency, λ is the phonon mode which consists of the wave vector and the phonon branch. Here, α and β indicate the Cartesian components. v is the phonon group velocity, and the term F is shown as

$$f_\lambda - f_0(\omega_\lambda) = -F_\lambda \cdot \Delta T \, df_0/dT, \tag{9}$$

which means that the phonon distribution f_λ deviates from the Bose-Einstein distribution $f_0(\omega_\lambda)$ when the temperature gradient ΔT is small enough in thermal equilibrium. Based on the kinetic theory, κ_L can be rewritten with the expression for mode level volumetric specific heat C_{ph}, phonon group velocity, and phonon relaxation time τ,

$$\kappa_L = \sum_{\vec{q}p} C_V v_\alpha(\vec{q}, p)^2 \tau(\vec{q}, p), \tag{10}$$

where v_α is the $\alpha(= x, y, z)$ component of v and $\vec{q}$ and p indicate wave vector and polarization, respectively.

III. RESULTS

A. Structure and phonon dispersion

The optimized structure of monolayer MX belongs to the $P\bar{6}m2$ (No. 187) space group symmetry with 4 atoms per unit cell. As shown in Figs. 1(a) and 1(b), the crystal exhibits a honeycomb structure, where two bonding M layers are sandwiched between two X layers, stacking in the X-M-M-X sequence. The optimized lattice parameters are 3.63, 3.82, and 4.08 Å for monolayer GaS, GaSe, and InSe, respectively, which are consistent with the previous reports[30–33] and presented in Table I along with other geometric parameters.

To verify the thermodynamical stabilities of these systems, the phonon dispersions are calculated, and InSe possesses a similar distribution to a previous report.[34] By diagonalizing the dynamical matrix, the calculated phonon dispersions along high-symmetry k-points and phonon density of states (DOS) of monolayer GaS, GaSe, and InSe are shown in Fig. 2. No imaginary frequencies are observed, which confirms the thermodynamical stabilities of these systems. There are 12 phonon branches corresponding to four atoms in the unit cell, including three acoustic phonon branches and nine optical phonon branches. The three lowest phonon branches are acoustic phonon branches, including an in-plane longitudinal

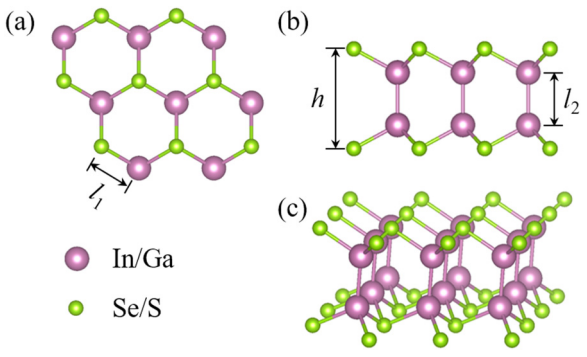

FIG. 1. The (a) top and [(b) and (c)] side views of the structure of monolayer MX (GaS, GaSe, and InSe).

TABLE I. Calculated lattice constant (a), thickness between top and bottom X layers (h), bond length of M–X (l_1) and M–M (l_2), volume specific heat (C_V), lattice thermal conductivity (κ_L), and atomic mass of unit cell (m).

	a (Å)	h (Å)	l_1 (Å)	l_2 (Å)	C_V (kJ m^{-3} K^{-1})	κ_L (W m^{-1} K^{-1})	m
GaS	3.64	4.66	2.37	2.47	1497.08	14.26	203.576
GaSe	3.82	4.83	2.5	2.47	1397.76	13.35	297.366
InSe	4.08	5.38	2.68	2.83	1261.78	2.69	387.556

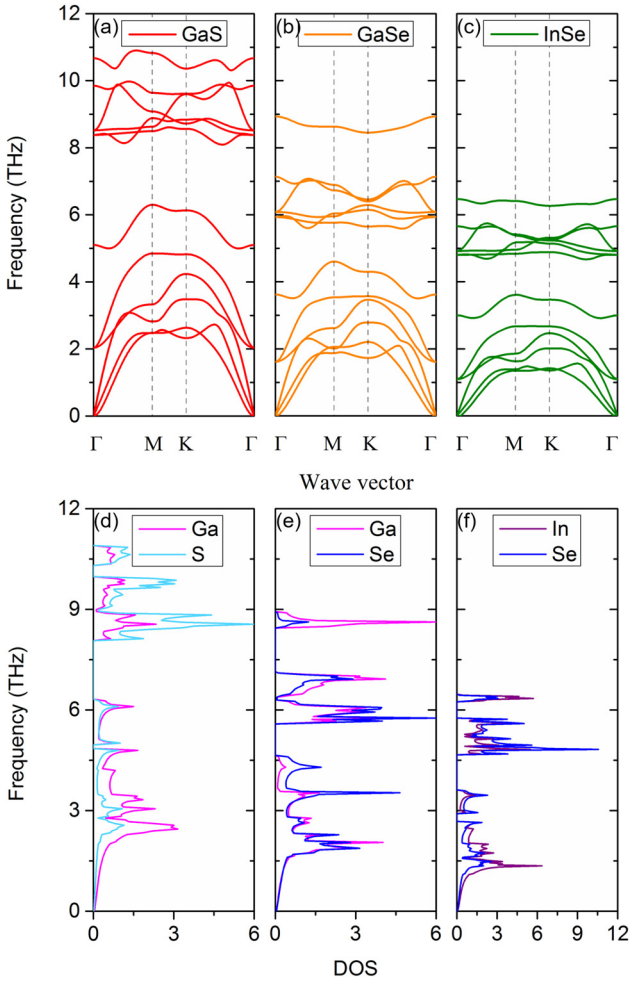

FIG. 2. The thermodynamical stability verified by the lattice vibrations properties. The phonon dispersion curves along the path passing through the high-symmetry k-points in the irreducible Brillouin zone (BZ) of (a) GaS, (b) GaSe, and (c) InSe with the corresponding partial density of states (DOS) of (d) GaS, (e) GaSe, and (f) InSe.

acoustic (LA), a transverse acoustic (TA) branch, and an out-of-plane (z-direction) flexural acoustic (ZA) branch. The two obvious phonon bandgaps between the optical phonon branches for each monolayer material could decrease the scattering probability between optical and acoustic phonon branches, which predominately contribute to thermal conductivity. The hybridization of the lowest optical and the highest acoustic phonon branches can result in more phonon scattering. Moreover, the softened phonon branch with decreasing frequencies is due to the increasing average atomic mass of each system, which reveals stronger anharmonicity. These factors could play a significant role in the thermal transport processes.

B. Electric properties

Based on the optimized structures with thermodynamical stability, the electronic band structure and density of states of 2D GaS, GaSe, and InSe are calculated along the high-symmetry points in the Brillouin zone as presented in Fig. 3. The contributions from the valence state of atoms for the 2D systems as revealed in our work show good consistency with previous study by Schlüter.[35] The upper valence bands are consistent with the peaks of bulk GaSe[36] ranging from −4 to 0 eV, which mainly correspond to the Ga–Se bond formed by the Se-p and Ga-p orbitals. However, the highest peak of valence bands for bulk GaSe corresponds to unoccupied antibonding bands of the Ga–Ga bond and gives rise to the isolated lowest conduction bands around 2 eV. Such behaviors are all obviously different from the hybridization between Se-p and Ga-p orbitals for the F peak and the hybridization between Se-p and Ga-s orbitals for the lowest conduction bands in atomic thick GaSe. It is rather unusual that the band at the bottom of the conduction band with a parabolic dispersion remains at the Brillouin zone center (Γ point), while the valence band maximum (VBM) shifts progressively away from Γ to the nearby k-points. The unusual shifting of the VBM corresponds to a Mexican-hat-like energy surface around the Γ point, which is also referred to as a Lifshitz transition, an electronic topological transition, or a camel-back dispersion.[37–39] Such behavior commonly appears along with a less number of layers, especially for the monolayer systems studied here. The Mexican-hat dispersion results in a high density of states (Fig. 3) and a van Hove singularity near the VBM.[40] Moreover, it can affect the thermoelectric performance[39] and the magnetoresponsive behavior in 2D materials.[41] The Mexican-hat of monolayer GaS is larger than that of GaSe, and that of InSe is the smallest. The reason may lie in the charge transfer driven by the electronegativity relation (Se < S, In < Ga), which occupies the p orbitals of the S or Se atom that dominates the top valence bands (Fig. 3). A bandgap is visible in each band structure plot, indicating the semiconducting characteristics of monolayer MX. The minimum of the conduction bands (CBM) situates at the Γ point, while the VBM lies between the Γ and k-points, indicating indirect bandgaps, while a direct gap semiconductor character was reported for bulk GaSe.[42] The calculated values of energy gaps between the lowest conduction band and the highest valance band are 3.05, 2.1, and 1.3 eV, which are consistent with previous research studies.[43–45] From the partial density of states of MX monolayers, both lower valence bands and lower conduction bands were mainly attributed to the M-s and X-p orbitals, implying the strong hybridization between them,

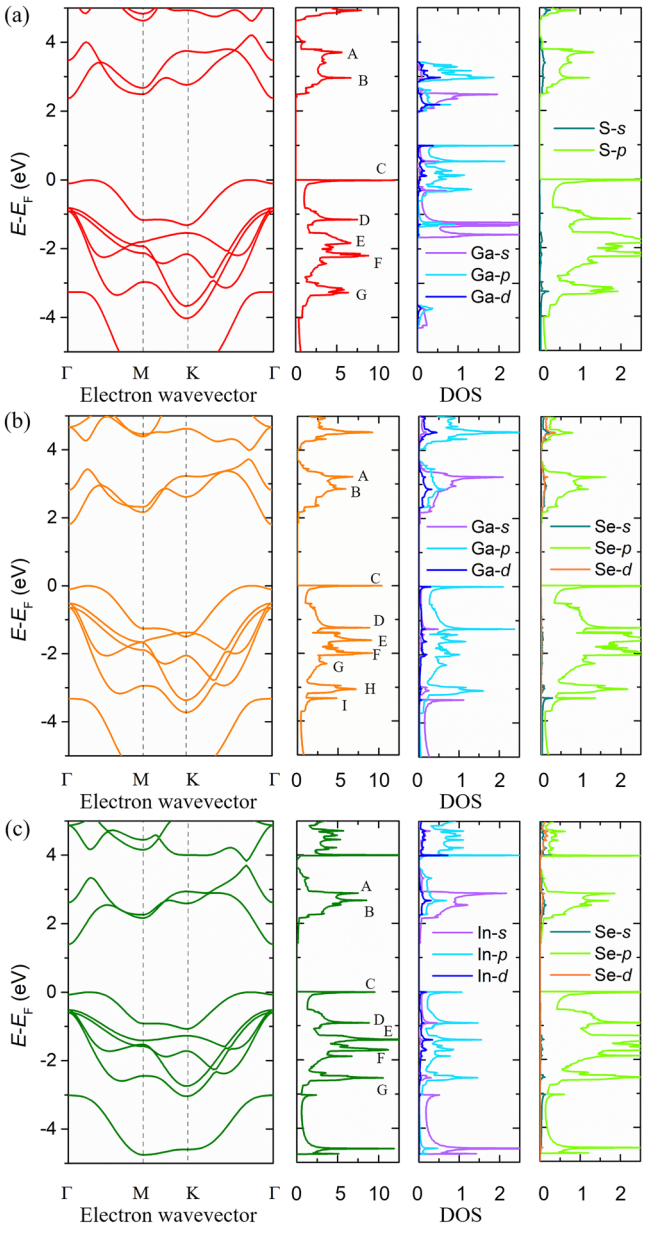

FIG. 3. The electronic properties. Calculated electronic structures along the high-symmetry k-points in the BZ for monolayer (a) GaS, (b) GaSe, and (c) InSe with the corresponding total and partial DOS.

while the upper valence bands and upper conduction bands were attributed to the hybridization of M-p and X-p orbitals. The M–M bonding force is covalent, and the M–X bonding force is both covalent and ionic. Based on the electronic band structures, insight into the possibility of electron's band-to-band transition and the interpretation of dielectric function spectra of monolayer MX could be obtained, which will be presented in Sec. III C.

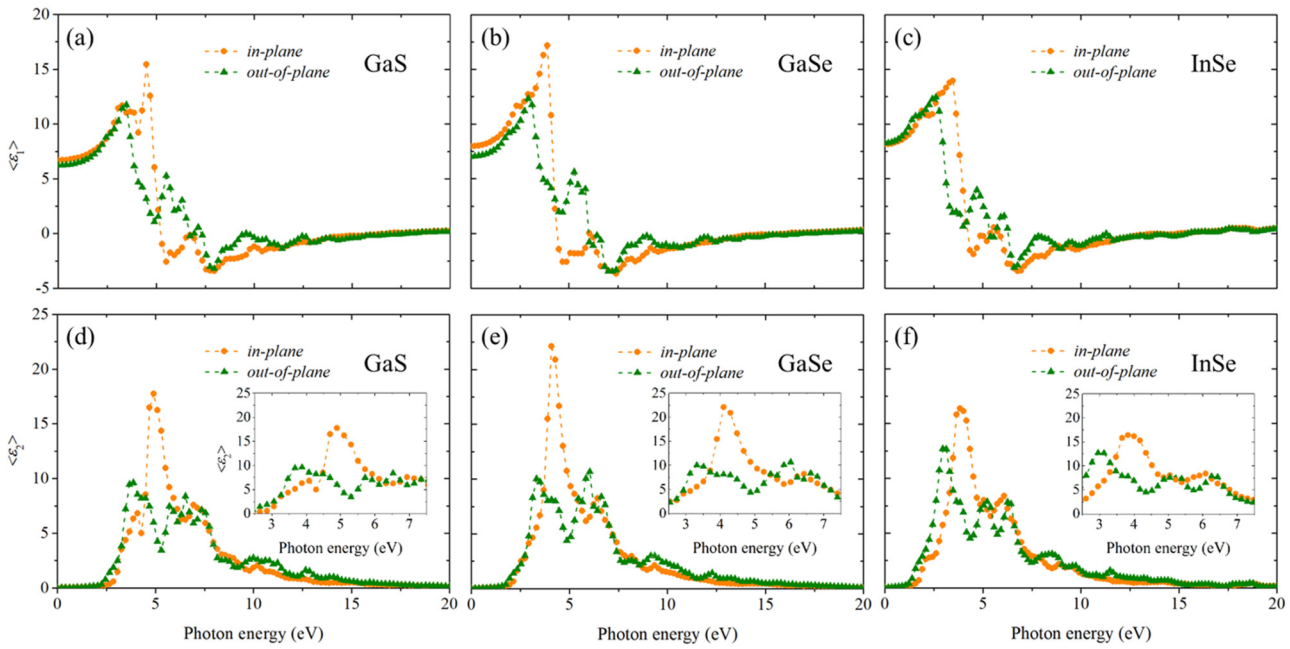

FIG. 4. Real part ε_1 of the dielectric function of monolayer (a) GaS, (b) GaSe, and (c) InSe, and imaginary part ε_2 of the dielectric function of monolayer (d) GaS, (e) GaSe, and (f) InSe.

C. Optical properties

The optical properties of materials can be revealed by the light absorption arising from the interaction between the light and the electrons or atoms, which is governed by the characteristics of the electronic band structures. To investigate the optical properties of the monolayer GaS, GaSe, and InSe, the dielectric functions are further calculated from first-principles in addition to the electronic structures. Energy-dependent real part ε_1 and imaginary part ε_2 of the normalized dielectric function of monolayer MX along in-plane and out-of-plane directions are plotted in Fig. 4. ε_1 and ε_2 of monolayer MX present in-plane isotropy, which is different from that of the out-of-plane direction. The anisotropy mainly arises from the two-dimensional character of monolayer MX. The absorption peak of ε_2 along in-plane and out-of-plane directions of monolayer GaS, GaSe, and InSe are listed in Table II. The appearance of the first peak in the in-plane direction of ε_2 for 2D GaS at 4.08 eV before the main peak at 4.89 eV is typical for ionic compounds. This peak originates from the existence of a "quasi-optical-gap" in the band structure, which is due to the forbidden transitions rather than a zero-point density of states.[46] The highest peak of ε_2 is in the order GaSe > GaS > InSe along the in-plane direction, and InSe > GaSe > GaS along the out-of-plane direction. Based on the band-to-band transition theory, absorption peak around photon energy in Table II can be fundamentally interpreted through the calculated intrinsic electronic band structure and density of states as indicated in Table III. It shows that the strongest peak of ε_2 along the in-plane direction [Figs. 4(d)–4(f)] around 4.89 eV of GaS is attributed to the E → B and D → A transitions, around 4.09 eV of GaSe is attributed to the D → B transition, and around 3.82 eV of InSe is attributed to the E → B and D → A transitions. Therefore, at higher photon energy, the interband transition dominates optical absorption. These peaks present a redshift from GaS to GaSe and then to InSe, because more electrons tend to occupy a higher energy state. For ε_2 along the out-of-plane direction [Figs. 4(d)–4(f)], the strongest absorption peaks centered around 3.87 eV of GaS and 2.95 eV of InSe could be contributed by the intraband transition. But for GaSe, the strongest absorption peaks centered around 6.04 eV is attributed to the I → B and H → A interband transitions, while the second strongest absorption peaks centered around 3.31 eV could be contributed by the intraband

TABLE II. Absorption peaks of ε_2 along the in-plane (//) and out-of-plane (⊥) directions of monolayer GaS, GaSe, and InSe.

	GaS		GaSe		InSe	
	E	ε_2	*E*	ε_2	*E*	ε_2
//	4.08	6.81	4.09	22.1	3.82	16.39
	4.89	17.74	6.43	8.24	6.08	8.38
	6.93	7.57				
⊥	3.87	9.61	3.31	10.03	2.95	12.69
	5.71	7.46	5.45	8.22	5.21	7.88
	6.52	8.37	6.04	10.67	6.25	7.82
	7.34	7.14	6.62	8.41		

TABLE III. Interband transition process corresponding to the absorption peaks of ε_2 along the in-plane (//) and out-of-plane (⊥) directions of monolayer GaS, GaSe, and InSe.

		Photon energy (eV)	Interband transition
GaS	//	4.08	D(−1.15 eV) → B(2.95 eV)
		4.89	E(−1.83 eV) → B(2.95 eV), D(−1.15 eV) → A(3.7 eV)
		6.93	G(−3.27 eV) → A(3.7 eV)
	⊥	5.71	E(−1.83 eV) → A(3.7 eV), F(−2.2 eV) → A(3.7 eV)
GaSe	//	4.09	D(−1.24 eV) → B(2.85 eV)
		6.43	I(−3.32 eV) → A(3.2 eV)
	⊥	5.45	G(−2.3 eV) → A(3.2 eV)
		6.04	I(−3.32 eV) → B(2.85 eV), H(−3.06 eV) → A(3.2 eV)
		6.62	I(−3.32 eV) → A(3.2 eV)
InSe	//	3.82	E(−1.41 eV) → B(2.67 eV), D(−0.91 eV) → A(2.88 eV)
	⊥	5.21	G(−2.52 eV) → B(2.67 eV)

transition. Like ε_2, ε_1 is also in-plane isotropic, and their strongest peak values are in the order GaSe > GaS > InSe along the in-plane direction and GaSe > InSe > GaS along the out-of-plane direction. When $\varepsilon_1 < 0$, the vector wave K is an imaginary number due to the vector wave equation $\omega^2\varepsilon = c^2(K \cdot K)$.

Normal-incidence reflectance R and optical absorption coefficient α can be obtained based on normalized dielectric functions.

TABLE IV. Absorption peaks of R and α along the in-plane (//) and out-of-plane (⊥) directions of monolayer GaS, GaSe, and InSe.

		E (eV)	R	E (eV)	α
GaS	//	7.96	0.34	7.55	1.624×10^5
	⊥	7.96	0.33	7.75	1.608×10^5
GaSe	//	7.41	0.54	7.41	2.574×10^5
	⊥	7.41	0.55	6.82	2.608×10^5
InSe	//	6.95	0.53	6.78	2.388×10^5
	⊥	6.78	0.49	6.61	2.325×10^5

The highest R and α of monolayer MX along both the in-plane and out-of-plane directions are provided in Table IV. The positions of the first reflectivity peaks for the 2D systems show a different behavior from the bulk systems. For example, the first peaks of monolayer GaSe are 4.28 and 3.31 eV for the in-plane and out-of-plane directions, respectively, which is quite different from the reflectivity of bulk GaSe with the first peak around 3.8 eV.[36] Note that the second peaks in both directions for 2D GaSe present a blue shift compared to that in bulk GaSe. Photon energy of maximum R and α slightly shifts to lower frequency from monolayer GaS to GaSe and then to InSe as shown in Fig. 5. The absorptivity of monolayer GaS, GaSe, and InSe in the visible band are about 1.41%, 2.28%, and 2.1% along in-plane, 1.4%, 2.31%, and 2.04% along out-of-plane, respectively; therefore, absorptivity is equal to the multiplication of absorption coefficient α and thickness d.[17]

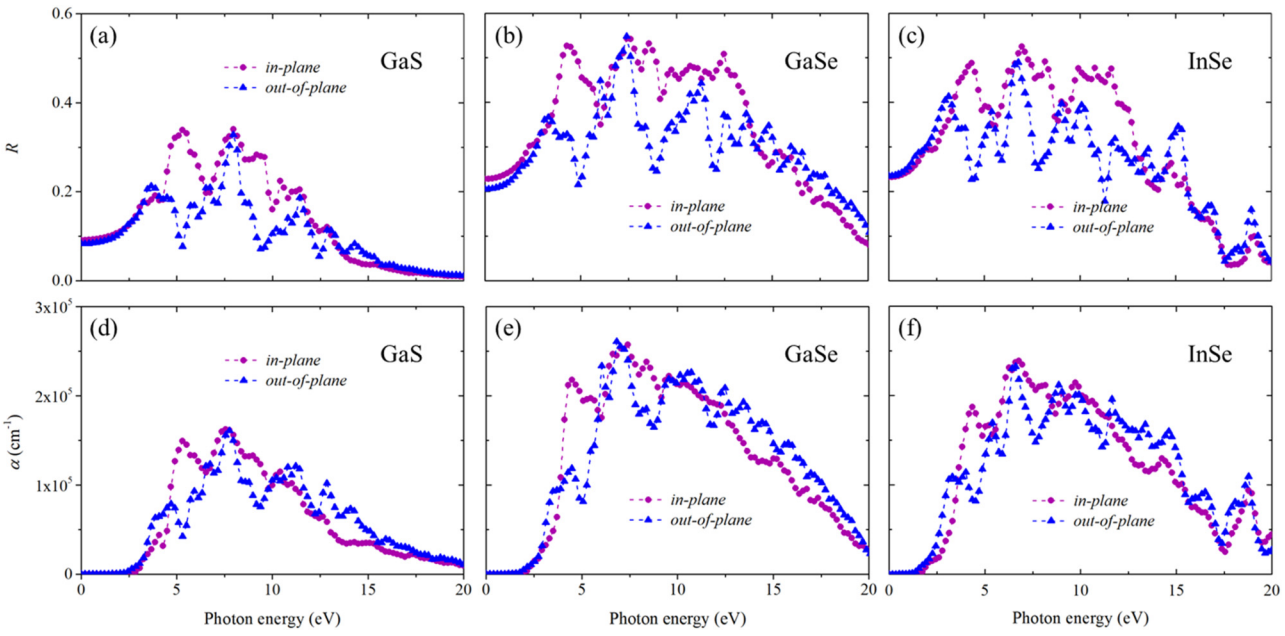

FIG. 5. Reflectivity $R(\omega)$ of monolayer (a) GaS, (b) GaSe, and (c) InSe, and absorption coefficient $\alpha(\omega)$ of monolayer (d) GaS, (e) GaSe, and (f) InSe.

D. Thermal transport properties

With the remarkable electronic and optical properties as analyzed above, the monolayer GaS, GaSe, and InSe show promising applications in photoelectrics. Since the thermal transport properties play a key role for efficient heat dissipation during the device operation, we further investigate the phonon thermal transport behavior of the monolayer GaS, GaSe, and InSe. By iteratively solving the phonon BTE based on first-principles calculations of the IFCs, the thermal conductivity of monolayer GaS, GaSe, and InSe are obtained as 14.26, 13.35, and 2.69 $Wm^{-1}K^{-1}$, respectively. The thermal conductivities of monolayer GaS, GaSe, and InSe are close to that of silicene and black phosphorene, which means that the thermal conductivities are sufficient for their applications as optoelectronic devices.

Based on previous studies, the thermal conductivity generally decreases with increasing atomic mass.[47] The decreased thermal conductivity from monolayer GaS and GaSe to InSe agrees well with the common knowledge. However, the decrease of thermal conductivity from GaS to GaSe is quite small (by 0.91 $Wm^{-1}K^{-1}$) compared to that from GaSe to InSe (by 10.66 $Wm^{-1}K^{-1}$), despite the almost equal mass difference (93.79 and 90.91, respectively) [Fig. 6(a)]. To achieve a fundamental understanding of the intriguing phenomena, we further perform a detailed analysis on the mode level information of phonon thermal transport. As shown in Fig. 6(b), the decrease of mode resolved thermal conductivity is consistent with the overall thermal conductivity, especially for the low-frequency phonons which dominate the thermal transport. It is clearly shown in Eq. (10) that the thermal conductivity is mainly determined by the group velocity and phonon relaxation time. The group velocity [Fig. 6(e)] is calculated based on the phonon dispersion [Figs. 2(a)–2(c)]. The group velocity shows an equal decrease from GaS and GaSe to InSe, which is consistent with the evolution of phonon dispersion. Thus, the large difference in the decrease of thermal conductivity from GaS and GaSe to InSe must lie in the unequal decrease of phonon relaxation time as shown in Fig. 6(d). Further analysis reveals that the underlying reason lies in the anomalous phonon anharmonicity as quantified by the Grüneisen parameter as shown in Fig. 6(c). The phonon anharmonicity in GaSe is anomalously weak compared to GaS and InSe, leading to larger phonon relaxation time and then larger thermal conductivity. Consequently, the decrease of thermal conductivity from GaS to GaSe is relatively small compared to that from GaSe to InSe as discussed above.

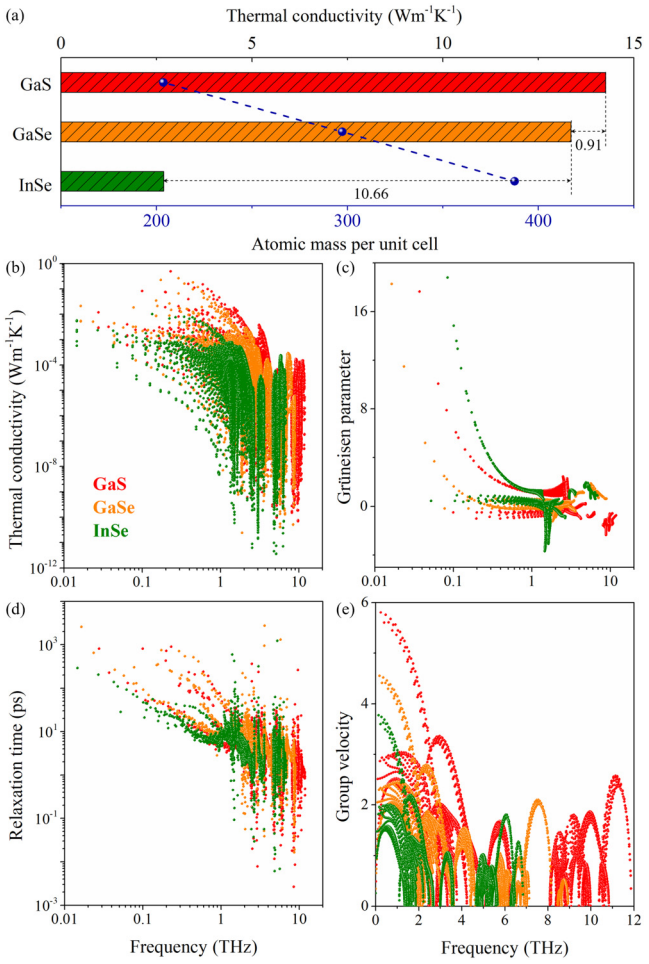

FIG. 6. Thermal transport properties. Comparison of (a) thermal conductivity, (b) mode level thermal conductivity, (c) mode level Grüneisen parameter, (d) mode level phonon relaxation time, and (e) mode level phonon group velocity between monolayer GaS, GaSe, and InSe at 300 K.

IV. CONCLUSION

We have systematically investigated the electronic, optical, and thermal transport properties of monolayer GaS, GaSe, and InSe based on first-principles calculations. The electric bands present unusual morphology as the parabolic bottom of the conduction and the flattop of the valence with indirect 3.05, 2.1, and 1.3 eV bandgap for GaS, GaSe, and InSe, respectively. ε_1 and ε_2 of these monolayers present in-plane isotropy from their two-dimensional characteristics. Based on the band-to-band transition theory, the strongest absorption peaks of ε_2 could be contributed by interband transitions except for those of GaS and InSe along the out-of-plane direction, which are attributed to the intraband transition. The highest peak of ε_2 along the in-plane direction presents a redshift from GaS and GaSe to InSe, due to more electrons occupying higher energy state. GaSe possesses the highest absorptivity with 2.31% along out-of-plane. Although these materials all have low lattice thermal conductivities, the decrease of thermal conductivity from GaS to GaSe is quite tiny (by 0.91 $Wm^{-1}K^{-1}$) compared to that from GaSe to InSe (by 10.66 $Wm^{-1}K^{-1}$), along with almost equal mass difference (93.79 and 90.91, respectively). Through mode level analysis, the unequal decrease of thermal conductivity from GaS and GaSe to InSe is due to the larger phonon relaxation time deriving from weaker phonon anharmonicity of GaSe than the other two. Our study provides a comprehensive understanding of the inherent properties in monolayer GaS, GaSe, and InSe for the photoelectric applications.

ACKNOWLEDGMENTS

Simulations were performed with the computing resources granted by the RWTH Aachen University (Project No. rwth0288).

H.W. is grateful for the fellowship support of the China Scholarship Council (CSC) (No. [2015]3022) and acknowledges the careful proofreading of the manuscript by Mr. Alejandro Rodriguez (University of South Carolina). This work was also financially supported by the National Natural Science Foundation of China (NNSFC) (Grant Nos. 51425401 and 11847158) and the China Postdoctoral Science Foundation (2018M642776). Research reported in this publication was supported in part by the NSF and SC EPSCoR/IDeA Program under NSF OIA-1655740 and SC EPSCoR/IDeA 19-SA06. G.Q. is supported by an ASPIRE grant from the Office of the Vice President for Research at the University of South Carolina.

REFERENCES

[1]K. Keyshar, Y. Gong, G. Ye, G. Brunetto, W. Zhou, D. Cole, K. Hackenberg, Y. He, L. Machado, M. Kabbani, A. Hart, B. Li, D. Galvao, A. George, R. Vajtai, C. Tiwary, and P. Ajayan, "Chemical vapor deposition of monolayer rhenium disulfide (ReS_2)," Adv. Mater. **27**, 4640–4648 (2015).
[2]N. Zhang, M.-Q. Yang, S. Liu, Y. Sun, and Y.-J. Xu, "Waltzing with the versatile platform of graphene to synthesize composite photocatalysts," Chem. Rev. **115**, 10307–10377 (2015).
[3]G. Xie, K. Zhang, B. Guo, Q. Liu, L. Fang, and J. R. Gong, "Graphene-based materials for hydrogen generation from light-driven water splitting," Adv. Mater. **25**, 3820–3839 (2013).
[4]P. Hu, L. Wang, M. Yoon, J. Zhang, W. Feng, X. Wang, Z. Wen, J. Idrobo, Y. Miyamoto, D. Geohegan, and K. Xiao, "Highly responsive ultrathin GaS nanosheet photodetectors on rigid and flexible substrates," Nano Lett. **13**, 1649–1654 (2013).
[5]Q. Wang, K. Zadeh, A. Kis, J. Coleman, and M. Strano, "Electronics and optoelectronics of two-dimensional transition metal dichalcogenides," Nat. Nanotechnol. **7**, 699–712 (2012).
[6]H. R. Jappor, "Electronic structure of novel GaS/GaSe heterostructures based on GaS and GaSe monolayers," Physica B **524**, 109–117 (2017).
[7]K. E. Glukhov and N. K. Tovstyuk, "Elementary energy bands concept, band structure, and peculiarities of bonding in β-InSe crystal," Phys. Status Solidi B **247**, 318–324 (2010).
[8]X. Zhang, S. Wang, G. Wan, Y. Zhang, M. Huang, and L. Yi, "Transient reflectivity measurement of photocarrier dynamics in GaSe thin films," Appl. Phys. B **123**, 86 (2017).
[9]K. Dani, J. Lee, R. Sharma, A. Mohite, C. Galande, P. Ajayan, A. Dattelbaum, H. Htoon, A. Taylor, and R. Prasankumar, "Intraband conductivity response in graphene observed using ultrafast infrared-pump visible-probe spectroscopy," Phys. Rev. B Condens. Matt. **86**, 125403 (2012).
[10]S. Gilbertson, G. L. Dakovski, T. Durakiewicz, J.-X. Zhu, K. M. Dani, A. D. Mohite, A. Dattelbaum, and G. Rodriguez, "Tracing ultrafast separation and coalescence of carrier distributions in graphene with time-resolved photoemission," J. Phys. Chem. Lett. **3**, 64–68 (2012).
[11]D. J. Late, B. Liu, J. Luo, A. Yan, H. S. S. R. Matte, M. Grayson, C. N. R. Rao, and V. P. Dravid, "Gas and GaSe ultrathin layer transistors," Adv. Mater. **24**, 3549–3554 (2012).
[12]S. Lei, L. Ge, S. Najmaei, A. George, R. Kappera, J. Lou, M. Chhowalla, H. Yamaguchi, G. Gupta, R. Vajtai, A. D. Mohite, and P. M. Ajayan, "Evolution of the electronic band structure and efficient photo-detection in atomic layers of InSe," ACS Nano **8**, 1263–1272 (2014).
[13]M. Mahjouri-Samani, M. Tian, K. Wang, A. Boulesbaa, C. M. Rouleau, A. A. Puretzky, M. A. McGuire, B. R. Srijanto, K. Xiao, G. Eres, G. Duscher, and D. B. Geohegan, "Digital transfer growth of patterned 2D metal chalcogenides by confined nanoparticle evaporation," ACS Nano **8**, 11567–11575 (2014).
[14]M. Mahjouri-Samani, R. Gresback, M. Tian, K. Wang, A. A. Puretzky, C. M. Rouleau, G. Eres, I. N. Ivanov, K. Xiao, M. A. McGuire, G. Duscher, and D. B. Geohegan, "Pulsed laser deposition of photoresponsive two-dimensional GaSe nanosheet networks," Adv. Funct. Mater. **24**, 6365–6371 (2014).
[15]D. Ma, W. Ju, Y. Tang, and Y. Chen, "First-principles study of the small molecule adsorption on the InSe monolayer," Appl. Surf. Sci. **426**, 244–252 (2017).
[16]D. A. Bandurin, A. V. Tyurnina, G. L. Yu, A. Mishchenko, V. Zólyomi, S. V. Morozov, R. K. Kumar, R. V. Gorbachev, Z. R. Kudrynskyi, S. Pezzini, Z. D. Kovalyuk, U. Zeitler, K. S. Novoselov, A. Patanè, L. Eaves, I. V. Grigorieva, V. I. Fal'ko, A. K. Geim, and Y. Cao, "High electron mobility, quantum Hall effect and anomalous optical response in atomically thin InSe," Nat. Nanotech. **12**, 223–227 (2017).
[17]J. Y. Yang and L. H. Liu, "Effects of interlayer screening and temperature on dielectric functions of graphene by first-principles," J. Appl. Phys. **120**, 034305 (2016).
[18]Z. M. Zhang, *Nano/Microscale Heat Transfer* (McGraw-Hill, New York, 2007).
[19]N. T. Hung, A. R. T. Nugraha, and R. Saito, "Two-dimensional InSe as a potential thermoelectric material," Appl. Phys. Lett. **111**, 092107 (2017).
[20]J.-S. Rhyee, K. H. Lee, S. M. Lee, E. Cho, S. I. Kim, E. Lee, Y. S. Kwon, J. H. Shim, and G. Kotliar, "Peierls distortion as a route to high thermoelectric performance in In_4Se_3-δ crystals," Nature **459**, 965–968 (2009).
[21]G. Kresse and J. Hafner, "Ab initio molecular dynamics for liquid metals," Phys. Rev. B **47**, 558–561 (1993).
[22]G. Kresse and J. Hafner, "Ab initio molecular-dynamics simulation of the liquid-metal–amorphous-semiconductor transition in germanium," Phys. Rev. B **49**, 14251–14269 (1994).
[23]G. Kresse and J. Furthmüller, "Efficient iterative schemes for ab initio total-energy calculations using a plane-wave basis set," Phys. Rev. B **54**, 11169–11186 (1996).
[24]P. E. Blöchl, "Projector augmented-wave method," Phys. Rev. B **50**, 17953–17979 (1994).
[25]G. Kresse and D. Joubert, "From ultrasoft pseudopotentials to the projector augmented-wave method," Phys. Rev. B **59**, 1758–1775 (1999).
[26]H. J. Monkhorst and J. D. Pack, "Special points for Brillouin-zone integrations," Phys. Rev. B **13**, 5188–5192 (1976).
[27]M. Gajdoš, K. Hummer, G. Kresse, J. Furthmüller, and F. Bechstedt, "Linear optical properties in the projector-augmented wave methodology," Phys. Rev. B **73**, 045112 (2006).
[28]H. Bao and X. Ruan, "Ab initio calculations of thermal radiative properties: The semiconductor GaAs," Int. J. Heat Mass Transfer **53**, 1308 (2010).
[29]W. Li, J. Carrete, N. A. Katcho, and N. Mingo, "ShengBTE: A solver of the Boltzmann transport equation for phonons," Comput. Phys. Commun. **185**, 1747–1758 (2014).
[30]A. S. Nissimagoudar, J. Ma, Y. Chen, and W. Li, "Thermal transport in monolayer InSe," J. Phys. Condens. Matter **29**, 335702 (2017).
[31]T. Pandey, D. S. Parker, and L. Lindsay, "*Ab initio* phonon thermal transport in monolayer InSe, GaSe, GaS, and alloys," Nanotechnology **28**, 455706 (2017).
[32]X. Li, C. Xia, X. Song, J. Du, and W. Xiong, "n- and p-type dopants in the InSe monolayer via substitutional doping," J. Mater. Sci. **52**, 7207–7214 (2017).
[33]Y. Ma, Y. Dai, M. Guo, L. Yu, and B. Huang, "Tunable electronic and dielectric behavior of GaS and GaSe monolayers," Phys. Chem. Chem. Phys. **15**, 7098–7104 (2013).
[34]V. Zólyomi, N. D. Drummond, and V. I. Fal'ko, "Electrons and phonons in single layers of hexagonal indium chalcogenides from *ab initio* calculations," Phys. Rev. B **89**, 205416 (2014).
[35]M. Schlüter, "The electronic structure of GaSe," Il Nuovo Cimento B **13**, 313 (1973).
[36]M. Schlüter, J. Camassel, S. Kohn, J. P. Voitchovsky, Y. R. Shen, and M. L. Cohen, "Optical properties of GaSe and GaS_xSe_{1-x} mixed crystals," Phys. Rev. B **13**, 3534–3547 (1976).
[37]V. Zólyomi, N. D. Drummond, and V. I. Fal'ko, "Band structure and optical transitions in atomic layers of hexagonal gallium chalcogenides," Phys. Rev. B **87**, 195403 (2013).

[38]A. Varlet, D. Bischoff, P. Simonet, K. Watanabe, T. Taniguchi, T. Ihn, K. Ensslin, M. Mucha-Kruczyński, and V. I. Fal'ko, "Anomalous sequence of quantum Hall liquids revealing a tunable Lifshitz transition in bilayer graphene," Phys. Rev. Lett. **113**, 116602 (2014).
[39]D. Wickramaratne, F. Zahid, and R. K. Lake, "Electronic and thermoelectric properties of van der Waals materials with ring-shaped valence bands," J. Appl. Phys. **118**, 075101 (2015).
[40]T. Cao, Z. Li, and S. G. Louie, "Tunable magnetism and half-metallicity in hole-doped monolayer GaSe," Phys. Rev. Lett. **114**, 236602 (2015).
[41]F. Li, X. Zhou, W. Feng, B. Fu, and Y. Yao, "Thickness-dependent magneto-optical effects in hole-doped GaS and GaSe multilayers: A first-principles study," New J. Phys. **20**, 043048 (2018).
[42]M. Yagmurcukardes, R. T. Senger, F. M. Peeters, and H. Sahin, "Mechanical properties of monolayer GaS and GaSe crystals," Phys. Rev. B **94**, 245407 (2016).
[43]D. J. Late, B. Liu, H. S. S. Ramakrishna Matte, C. N. R. Rao, and V. P. Dravid, "Rapid characterization of ultrathin layers of chalcogenides on SiO_2/Si substrates," Adv. Funct. Mater. **22**, 1894–1905 (2012).
[44]T. Hu, J. Zhou, and J. Dong, "Strain induced new phase and indirect–direct band gap transition of monolayer InSe," Phys. Chem. Chem. Phys. **19**, 21722–21728 (2017).
[45]S. Demirci, N. Avazlı, E. Durgun, and S. Cahangirov, "Structural and electronic properties of monolayer group III monochalcogenides," Phys. Rev. B **95**, 115409 (2017).
[46]G. Martinez, M. Schlüter, and M. L. Cohen, "Electronic structure of PbSe and PbTe II. Optical properties," Phys. Rev. B **11**, 660–670 (1975).
[47]H. Wang, G. Qin, G. Li, Q. Wang, and M. Hu, "Unconventional thermal transport enhancement with large atom mass: A comparative study of 2D transition dichalcogenides," 2D Mater. **5**, 015022 (2018).